

Scalar and Tensor Glueballs on Asymmetric Coarse Lattices

C. Liu^{a*}

^aDepartment of Physics, Peking University, Beijing 100871, P. R. China

Scalar and tensor glueball spectrum is studied using an improved gluonic action on asymmetric lattices in the pure $SU(3)$ gauge theory. The smallest spatial lattice spacing is about $0.08fm$ which makes the extrapolation to the continuum limit more reliable. In particular, attention is paid to the scalar glueball mass which is known to have problems in the extrapolation. Converting our lattice results to physical units using the scale set by the static quark potential, we obtain the following results for the glueball masses: $M_G(0^{++}) = 1730(90)MeV$ for the scalar glueball mass and $M_G(2^{++}) = 2400(95)MeV$ for the tensor glueball.

1. INTRODUCTION

It is believed that QCD is the theory which describes strong interactions among quarks and gluons. A direct consequence of this is the existence of excitations of pure gluonic degrees of freedom, i.e. glueballs. However, due to their non-perturbative nature, the spectrum of glueballs can only be investigated reliably with non-perturbative methods like lattice QCD [1–6]. Recently, it has become clear that such a calculation can be performed on a relatively coarse lattice using an improved gluonic action on asymmetric lattices [7–9]. In this paper, we present our results on lowest scalar and tensor glueball spectrum calculation. The spatial lattice spacing in our simulations ranges from $0.08fm$ to $0.25fm$ which enables us to extrapolate more reliably to the continuum limit. The improved gluonic action we used is the tadpole improved gluonic action on asymmetric lattices as described in [8,9]. It is given by:

$$S = - \beta \sum_{i>j} \left[\frac{5}{9} \frac{Tr P_{ij}}{\xi u_s^4} - \frac{Tr R_{ij}}{36 \xi u_s^6} - \frac{Tr R_{ji}}{36 \xi u_s^6} \right] - \beta \sum_i \left[\frac{4}{9} \frac{\xi Tr P_{0i}}{u_s^2} - \frac{1}{36} \frac{\xi Tr R_{i0}}{u_s^4} \right]. \quad (1)$$

*Work supported by the Chinese Natural Science Foundation under Grant No. 19705001, the Climb-up Fund from Ministry of Science and Technology and the Startup fund from Peking University.

In the above expression, β is related to the bare gauge coupling, $\xi = a_s/a_t$ is the (bare) aspect ratio of the asymmetric lattice with a_s and a_t being the lattice spacing in spatial and temporal direction respectively. The parameter u_s is the tadpole improvement parameter to be determined self-consistently from the spatial plaquettes in the simulation. P_{ij} and P_{0i} are the spatial and temporal plaquette variables. R_{ij} designates the 2×1 Wilson loop (2 in direction i and 1 in direction j). Using spatially coarse and temporally fine lattices helps to enhance signals in the glueball correlation functions. Therefore, the bare aspect ratio is taken to be some value larger than one. In our simulation, we have used $\xi = 3$ for our glueball calculation. It turns out that, using the non-perturbatively determined tadpole improvement [10] parameter u_s , the renormalization effects of the aspect ratio is small [8,9], typically of the order of a few percent for practical values of β in the simulation, which is ignored in this paper.

2. MONTE CARLO SIMULATIONS

We have utilized a Hybrid Monte Carlo algorithm to update gauge field configurations. Several lattice sizes have been simulated and the detailed information can be found in Table.1. For each lattice with fixed bare parameters, order of a few thousand configurations have been accumulated. Each gauge field configuration is separated from the previous one by several Hybrid

Table 1

Simulation parameters and the corresponding lattice spacing in physical units obtained from Wilson loop measurements. Parameters used in the smearing process for Wilson loop measurements are also listed.

Lattices	β	λ_W	n_W	r_0/a_s
$8^3 \times 24$	2.4	0.20 ~ 0.40	2 ~ 4	1.98(2)
$8^3 \times 24$	2.6	0.20 ~ 0.40	2 ~ 4	2.48(2)
$8^3 \times 24$	3.0	0.20 ~ 0.40	4 ~ 6	4.11(4)
$8^3 \times 24$	3.2	0.25 ~ 0.50	4 ~ 6	5.89(8)
$10^3 \times 30$	3.2	0.25 ~ 0.50	4 ~ 6	5.89(8)

Monte Carlo trajectories, typically 5 ~ 10, to make sure that they are sufficiently de-correlated. Further binning of the data has been performed and no noticeable remaining autocorrelation has been observed.

2.1. Setting the scale

In our simulation, the scale is set by measuring Wilson loops from which the static quark anti-quark potential $V(R)$ is obtained. Using the static potential between quarks, we are able to determine the lattice spacing in physical units by measuring r_0 , a pure gluonic scale determined from the static potential [11]. The definition of the scale r_0 is given by: $R^2 dV(R)/dR|_{R=r_0} = 1.65$. In physical units, r_0 is roughly $0.5 fm$ which is determined by comparison with potential models. For a recent determination of r_0 , please consult Ref. [12].

In order to measure the Wilson loops accurately, it is the standard procedure to perform single link smearing [2,8] on the spatial links and to utilize thermally averaged temporal links of the configurations. The smearing scheme can be performed iteratively on the spatial links of gauge fields for as many as n_W times with a smearing parameter λ_W . The smearing parameters λ_W and n_W used in this process are also listed in Table. 1. Wilson loops are then constructed using these smeared spatial links and thermally averaged temporal links. For a Wilson loop of size

$R \times T$, it is fitted against:

$$W(R, T) \stackrel{T \rightarrow \infty}{\sim} Z(R) e^{-V(R)T} . \quad (2)$$

The static quark potential $V(R)$ is obtained from the effective mass plateau in temporal direction. Wilson loops measured along different lattice axis and at different lattice spacings are seen to lie on a universal line which is an indication that the improved action restores the rotational symmetry quite well.

The static quark potential is fitted according to a Coulomb term plus a linear confining potential which is known to work well at these lattice spacings [9]. The potential is parameterized as:

$$V(R) = V_0 + e_c/R + \sigma R . \quad (3)$$

From this and the definition of r_0 , it follows that:

$$r_0/a_s = \sqrt{\frac{1.65 + e_c}{\sigma a_s^2}} . \quad (4)$$

To convert the measured result to r_0/a_s , we have also used the value of ξ taken as the bare value. The results of the spatial lattice spacing in physical units are also included in Table. 1. The errors for the ratio r_0/a_s are obtained by blocking the whole data set into smaller blocks and extracting the error from different blocks.

2.2. Glueball mass measurement

To obtain glueball mass values, it is necessary to construct glueball operators in various symmetry sectors of interests. Scalar glueball is in the A_1 representation of the cubic group; tensor glueball is in representation $E + T_2$, which forms a 5-dimensional representation; vector glueballs are in the representation T_1 [13,3].

Glueball correlation functions are noisy and difficult to measure. In order to enhance the signal of glueball correlation functions, smearing and fuzzifying have to be performed on spatial links of the gauge fields [2,8,9]. These techniques greatly enhance the overlap of the glueball states and thus provide possibility of measuring the mass values. The smearing and fuzzifying process involves typically 6 – 12 single link smearings plus a double link fuzzifying. In our simulations, after performing single link smearing

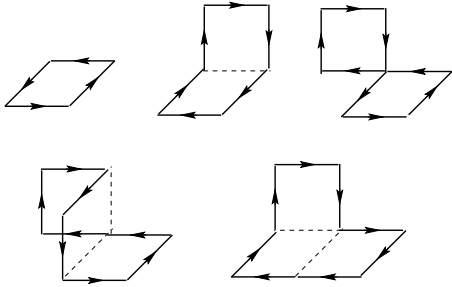


Figure 1. The Wilson loop shapes used in constructing the glueball operators.

and double link fuzzing on spatial links, we first construct raw operators at a given time slice t : $\{\mathcal{R}_t^{(i)} = \sum_{\mathbf{x}} \mathcal{W}_{\mathbf{x},t}^{(i)}\}$, where $\mathcal{W}_{t,\mathbf{x}}^{(i)}$ are closed Wilson loops originates from a given lattice point $x = (t, \mathbf{x})$. The loop-shapes studied in this calculation are shown in Fig.1. Then, elements from the cubic group is applied to these raw operators and the resulting set of loops now forms a basis for a representation of the cubic group. Suitable linear combinations of these operators are constructed to form a basis for a particular irreducible representation of interest [3]. We denote these operators as $\{\mathcal{O}_\alpha^{(R)}(t)\}$ where R labels a specific irreducible representation and α labels different operators at a given time slice t .

In order to maximize the overlap with one glueball state, we construct a glueball operator $\mathcal{G}^{(R)}(t) = \sum_\alpha v_\alpha^{(R)} \bar{\mathcal{O}}_\alpha^{(R)}(t)$, where $\bar{\mathcal{O}}_\alpha^{(R)}(t) = \mathcal{O}_\alpha^{(R)}(t) - \langle 0 | \mathcal{O}_\alpha^{(R)}(t) | 0 \rangle$. The coefficients $v_\alpha^{(R)}$ are determined from a variational calculation. To do this, we construct the correlation matrix:

$$\mathbf{C}_{\alpha\beta}(t) = \sum_\tau \langle 0 | \bar{\mathcal{O}}_\alpha^{(R)}(t + \tau) \bar{\mathcal{O}}_\beta^{(R)}(\tau) | 0 \rangle . \quad (5)$$

The coefficients $v_\alpha^{(R)}$ are chosen such that they minimize the effective mass

$$m_{eff}(t_C) = -\frac{1}{t_C} \log \left[\frac{v_\alpha^{(R)} v_\beta^{(R)} \mathbf{C}_{\alpha\beta}(t_C)}{v_\alpha^{(R)} v_\beta^{(R)} \mathbf{C}_{\alpha\beta}(0)} \right] , \quad (6)$$

where t_C is time separation for the optimization and repeated indices are summed over. In our

simulation $t_C = 1$ is taken. If we denote the optimal values of $v_\alpha^{(R)}$ by a column vector $\mathbf{v}^{(R)}$, this minimization is equivalent to the following eigenvalue problem:

$$\mathbf{C}(t_C) \cdot \mathbf{v}^{(R)} = e^{-t_C m_{eff}(t_C)} \mathbf{C}(0) \cdot \mathbf{v}^{(R)} . \quad (7)$$

The eigenvector $\mathbf{v}_0^{(R)}$ with the lowest effective mass then yields the coefficients $v_{0\alpha}^{(R)}$ for the operator $\mathcal{G}_0^{(R)}(t)$ which best overlaps the lowest lying glueball in the channel with symmetry R . Higher-mass eigenvectors of this equation will then overlap predominantly with excited glueball states of a given symmetry channel.

With these techniques, the glueball mass values are obtained in lattice units and the final results

Table 2

Glueball mass estimates for the symmetry channel A_1^{++} , E^{++} and T_2^{++} at various lattice spacings. The entries corresponding to the highest β value are the values after the infinite volume extrapolation. The last row tabulated the continuum extrapolated result of the glueball mass values in units of $1/r_0$.

β	$a_t M_{A_1^{++}}$	$a_t M_{E^{++}}$	$a_t M_{T_2^{++}}$
2.4	0.552(8)	0.980(10)	1.002(9)
2.6	0.482(12)	0.760(16)	0.798(15)
3.0	0.322(8)	0.460(13)	0.470(13)
3.2	0.233(7)	0.323(12)	0.340(10)
∞	4.23(22)	5.77(34)	5.92(32)

are listed in Table.2. The errors are obtained by binning the total data sets into several blocks and doing jackknife on them.

2.3. Extrapolation to the continuum limit

Finite volume errors are eliminated by performing simulations at the same lattice spacing but different physical volumes. This also helps to purge away the possible tolon states whose energy are sensitive to the size of the volume. A simulation at a larger volume is done for the smallest lattice spacing in our calculation. We found

that the mass of the scalar glueball remains unchanged when the size of the volume is increased. The mass of the tensor glueball is affected, which is consistent with the known result that tensor glueballs have a rather large size and therefore feel the finiteness of the volume more heavily. The infinite volume is obtained by extrapolating the finite volume results using the relation [14]:

$$a_t M^{(R)} = a_t M_\infty^{(R)} \left(1 - \frac{\lambda^{(R)}}{z} \exp\left(-\frac{\sqrt{3}z}{2}\right) \right), \quad (8)$$

where $z = M_\infty^{(A_1^{++})} L_s$. Using the results for the mass of the E^{++} and T_2 glueballs on $8^3 24$ and $10^3 30$ lattices for the same value of β , the final result for the mass of these glueball states are obtained. Glueball mass values for other symmetry sectors are not sensitive to the finite volume effects. Therefore, in Table.2, only the extrapolated values for the smallest physical volume are tabulated. Other entries are obtained from $8^3 24$ lattice results.

As for the finite lattice spacing errors, special attention is paid to the scalar glueball sector where the continuum limit extrapolation was known to have problems. Due to the simulation points at small lattice spacings, around $0.1 fm$ and below, the ambiguity in this extrapolation is reduced. We have tried to extrapolate the result using different formula suggested in Ref. [9], the extrapolated results are all consistent within statistical errors. For definiteness, we take the simple form:

$$M_G(a_s) = M_G(0) + \frac{c_1}{r_0} \left(\frac{a_s}{r_0}\right)^2 + \frac{c_2}{r_0} \left(\frac{a_s}{r_0}\right)^4, \quad (9)$$

and the result is illustrated in Fig.2. The final extrapolated results for the glueball mass values are also listed in Table.2. The data points from our simulation results are shown with solid symbols and the corresponding extrapolations are plotted as solid lines. It is also noticed that the extrapolated mass values for E^{++} and T_2^{++} channels coincide within statistical errors, indicating that in the continuum limit, they form the tensor representation of the rotational group. For comparison, corresponding results from [8] are also shown with open symbols and the dashed lines. If one

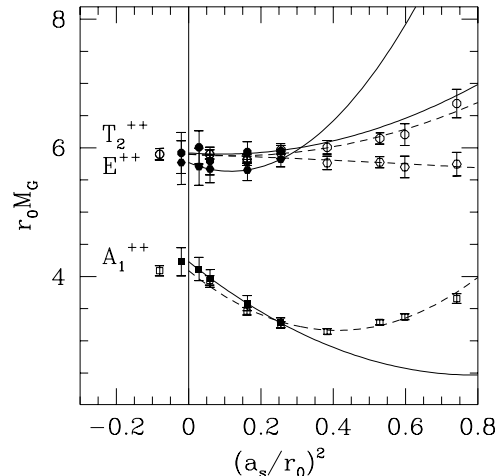


Figure 2. The continuum limit extrapolation of glueball mass values in scalar and tensor channels. The solid symbols are results from this calculation with the corresponding continuum limit extrapolation represented by the solid lines. For comparison, the corresponding results from [8,9] are also shown with open symbols and dashed lines.

would extrapolate linearly in $(a_s/r_0)^2$ using three data points with smallest lattice spacing, the results are statistically consistent with the results using the extrapolation (9) within errors. Our final extrapolated result for the scalar glueball mass lies higher, though still statistically consistent, than that of Ref.7. This has to do with the fact that simulation results at small lattice spacings are higher than those at larger lattice spacings. If one would extrapolate linearly using only the two data points with the smallest lattice spacing from [8,9], one would arrive at a higher scalar glueball mass value and closer to our result. This indicates that the difference between our final result on the scalar glueball mass and that of [8,9] basically comes from the ambiguity of the extrapolation when one tries to include more

data points from larger lattice spacings. In our calculation, with the help of one more point at smaller lattice spacing, using three data points with smallest lattice spacings, one can extrapolate linearly towards the continuum and obtain a result consistent with the result using a quadratic extrapolation. In the tensor channel, a constant extrapolation will also yield a consistent result. It is seen that, due to data points at lattice spacings around $0.1fm$ and below, the uncertainties in the extrapolation for the glueball mass values are reduced.

Finally, to convert our simulation results on glueball masses into physical units, we use the result $r_0^{-1} = 410MeV$. The errors for the hadronic scale r_0 is neglected. For the scalar glueball we obtain $M_G(0^{++}) = 1730(90)MeV$. For the tensor glueball mass in the continuum, we combine the results for the T_2^{++} and E^{++} channels and obtain $M_G(2^{++}) = 2400(95)MeV$ for the tensor glueball mass.

3. DISCUSSIONS AND CONCLUSIONS

We have studied the glueball spectrum at zero momentum in the pure $SU(3)$ gauge theory using Monte Carlo simulations on asymmetric lattices with the lattice spacing in the spatial directions ranging from $0.08fm$ to $0.25fm$. This helps to make extrapolations to the continuum limit with more confidence for the scalar and tensor glueball states. The mass values of the glueballs are converted to physical units in terms of the hadronic scale r_0 . We obtain the mass for the scalar glueball and tensor glueball to be: $M_G(0^{++}) = 1730(90)MeV$ and $M_G(2^{++}) = 2400(95)MeV$. It is interesting to note that, around these two mass values, experimental glueball candidates exist. Of course, in order to compare with the experiments other issues like the mixing effects and the effects of quenching have to be studied.

REFERENCES

1. G. Bali *et al.*, Phys. Lett. B **309**, 378 (1993).
2. C. Michael and M. Teper, Nucl. Phys. B **314**, 347 (1989).
3. B. Berg and A. Billoire, Nucl. Phys. B **221**, 109 (1983).
4. B. Berg and A. Billoire, Nucl. Phys. B **226**, 405 (1983).
5. K. Ishikawa, M. Teper and G. Schierholz, Phys. Lett. B **110**, 399; *ibid* Phys. Lett. B **116**, 429 (1982).
6. K. Ishikawa, A. Sato, G. Schierholz and M. Teper Z. Phys. C **21**, 167 (1983).
7. M. Alford *et al.*, Phys. Lett. B **361**, 87 (1995).
8. C. Morningstar and M. Peardon, Phys. Rev. D **56**, 4043 (1997).
9. C. Morningstar and M. Peardon, Phys. Rev. D **60**, 034509 (1999).
10. G. P. Lepage and P. B. Mackenzie, Phys. Rev. D **48**, 2250 (1993).
11. R. Sommer, Nucl. Phys. B **411**, 839 (1994).
12. M. Guagnelli, R. Sommer, and H. Wittig, Nucl. Phys. B **535**, 389 (1998).
13. R. C. Johnson, Phys. Lett. B **114**, 147 (1982).
14. M. Lüscher, Commun. Math. Phys. **104**, 177 (1986).